

Subtle Fluorination of Conjugated Molecules Enables Stable Nanoscale Assemblies on Metal Surfaces

Jens Niederhausen^{1,2,3}, Yuan Zhang¹, Fairoja Cheenicode Kabeer⁴, Yves Garmshausen⁵, Bernd M. Schmidt⁶, Yang Li¹, Kai-Felix Braun¹, Stefan Hecht⁵, Alexandre Tkatchenko^{4,7}, Norbert Koch^{2,3*}, and Saw-Wai Hla^{1,8,*}

¹*Nanoscale and Quantum Phenomena Institute, Physics & Astronomy Department, Ohio University, Athens, Ohio, 45701, USA.*

²*Institut für Physik & IRIS Adlershof, Humboldt-Universität zu Berlin, 12489 Berlin, Germany.*

³*Helmholtz-Zentrum Berlin für Materialien und Energie GmbH, 12489 Berlin, Germany.*

⁴*Fritz-Haber-Institut der Max-Planck-Gesellschaft, 14195 Berlin, Germany.*

⁵*Institut für Chemie & IRIS Adlershof, Humboldt-Universität zu Berlin, 12489 Berlin, Germany.*

⁶*Institute of Organic and Macromolecular Chemistry, Heinrich-Heine-University Düsseldorf, 40225 Düsseldorf, Germany*

⁷*Physics and Materials Science Research Unit, University of Luxembourg, L-1511 Luxembourg*

⁸*Center for Nanoscale Materials, Argonne National Laboratory, Argonne, IL, 60439, USA.*

*Correspondence email: norbert.koch@physik.hu-berlin.de; hla@ohio.edu

Additional first-principles electronic structure calculations for dimers with non-integer stack shift

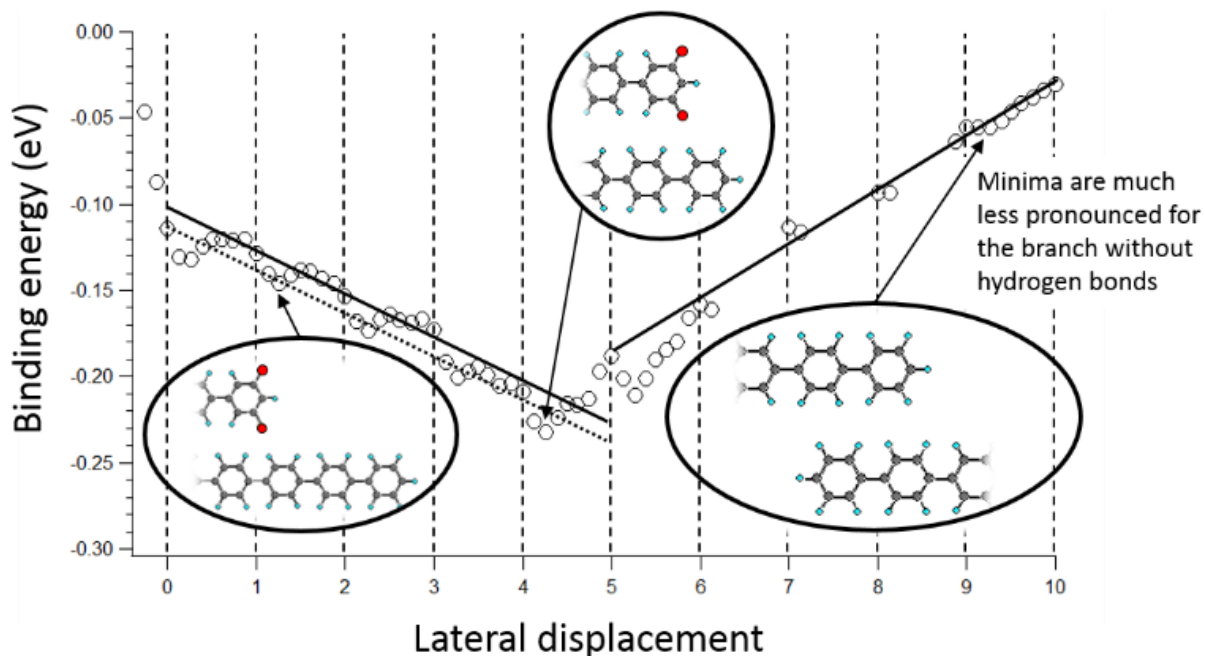


Figure S1. Binding energies as function of stack-shift, including non-integer multiples of the ring-to-ring distance for *m*-2F-6P.

In all calculations used for the main manuscript, the molecule that was moved ring-by-ring along the fixed another molecule was rotated by 180° about its long molecular axis every other ring to guarantee a similar geometry for two adjacent rings of the two different molecules and to provide maximal comparability. In contrast, Fig. S1 shows calculated structures for which no 180° rotations were applied, in order to more realistically map the binding energy evolution also for non-integer stack-shifts. Different from those presented in the main manuscript, these calculations were done with Gaussian09 (Revision A.02) using the PBE0 hybrid exchange-correlation functional and a 6-31G** contracted-Gaussian basis set.

Visualization of on-surface structures

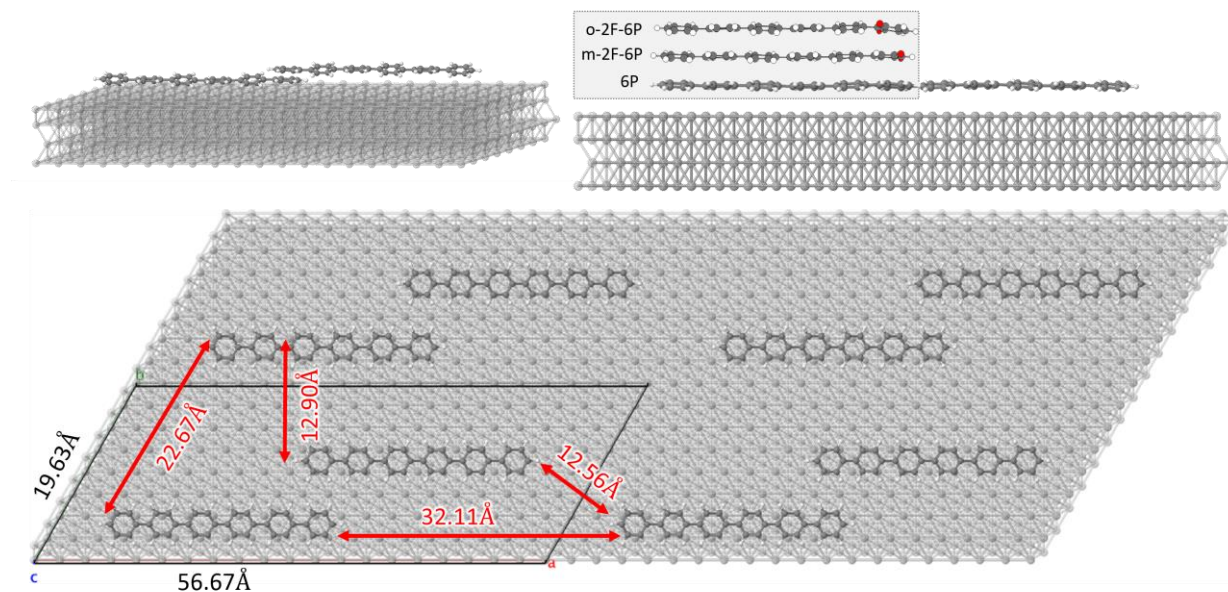


Figure S2: Top: Side views of 6P on Ag(111) in configuration (0). The right image also includes the side view of *o*-2F-6P and *m*-2F-6P. **Bottom:** Top view of the slab repeated along x and y directions. The distances between 6P molecules and the supercell dimensions are indicated.

Lattice parameter for Ag = 4.007 Å. Used 20x8 supercell of Ag surface with periodic boundary conditions having 4 metallic layers and vacuum of 40 Å.

Relaxed versus single point calculations

Table S1: Comparison between relaxed and non-relaxed (single point) studies for a *m*-2F-6P dimer in configuration (0) on Ag(111).

	PBE	
	relaxed	single point
Total energy of monomer [eV]	-43152.52687432	-43152.25219080
Total energy of Ag surface [eV]	-93688076.91339375	-93688073.28221993
Total energy of dimer/Ag system [eV]	-93774379.89637797	-93774376.39442636
Binding energy [eV]	2.071	1.392
Hirshfeld charge transfer	0.072	0.078

	PBE + vdW	
	relaxed	single point
Total energy of monomer [eV]	-43153.41787204	-43153.10561982
Total energy of Ag surface [eV]	-93688603.01372747	-93688602.9850630
Total energy of dimer/Ag system [eV]	-93774917.65883262	-93774916.85590017
Binding energy [eV]	-7.809	-7.660
vdW contribution	-9.880	-9.052

Interaction energies for 6P dimer formation on Ag(111)

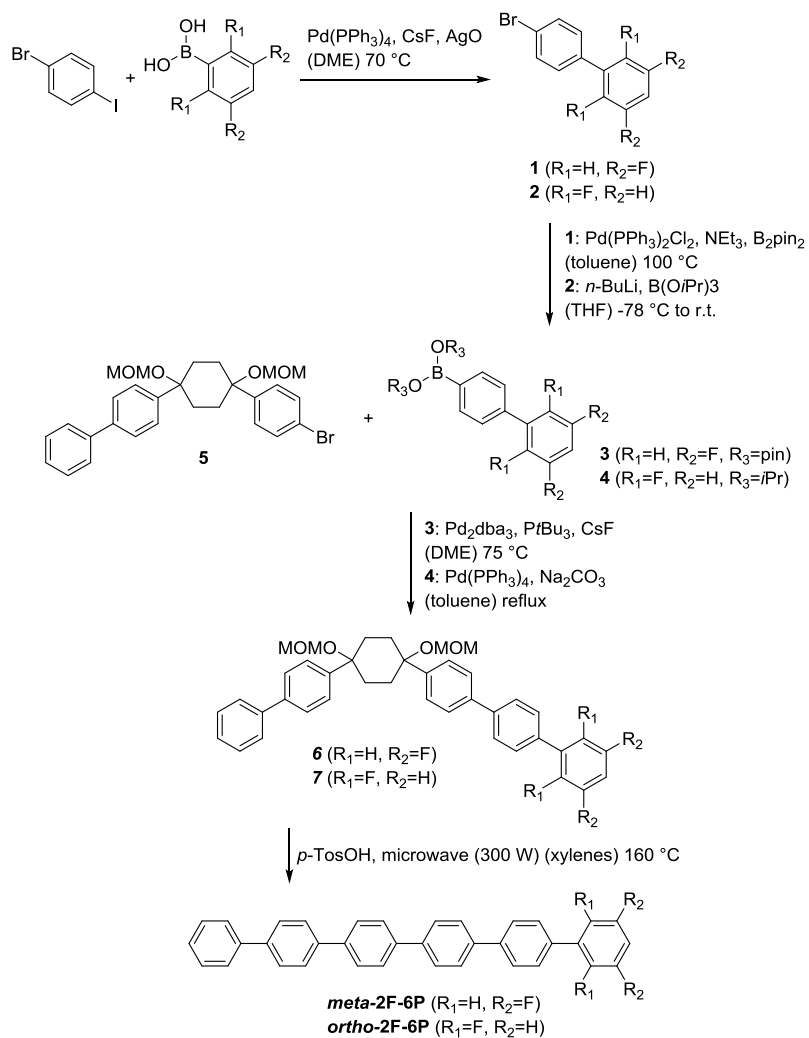
Table S2. Interaction energies for on-surface 6P dimer formation calculated with PBE+MBD according to binding energy of dimer on Ag(111) - 2 * binding energy of monomer on Ag(111), where binding energy of monomer on Ag(111) = -5.8848 eV

Configuration	Binding energy of dimer on Ag(111) [eV]	Interaction energy [eV]
0	-5.8244	0.0604
1	-5.8062	0.0786
2	-5.7782	0.1066
3	-5.7725	0.1123
4	-5.7541	0.1307
5	-5.7702	0.1146
6	-5.7638	0.1210
7	-5.7807	0.1041
8	-5.7893	0.0955
9	-5.8124	0.0724
10	-5.8420	0.0428

General synthetic and analytical methods

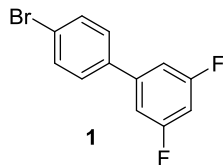
Solvents (ethyl acetate, tetrahydrofuran, dichloromethane, petroleum ether, toluene, ethanol, and methanol) were distilled before usage. All other starting materials were used as received from Sigma-Aldrich, Fischer-Scientific, TCI, and ABCR. Dry solvents were taken from a Pure Solv Micro Solvent Purification System. The intermediate building block 1-(4-bromophenyl)-4-(biphenyl-4-yl)-1,4-bis(methoxymethoxy)cyclohexane was described earlier.¹ Microwave irradiations were performed using a CEM Discover microwave. Fluorescence spectra were recorded on a Cary Eclipse fluorescence spectrometer using spectroscopy grade chloroform at 25 °C. NMR spectra were recorded on a Bruker DPX 300 Spectrometer (300 MHz for ¹H, 75 MHz for ¹³C, and 282 MHz for ¹⁹F) at 25 °C using residual protonated solvent signals as internal standard (¹H: $\delta(\text{CHCl}_3) = 7.26$ ppm; $\delta(\text{CH}_2\text{Cl}_2) = 5.32$ ppm; $\delta(\text{DMSO-d}_5) = 2.50$ ppm; ¹³C: $\delta(\text{CDCl}_3) = 77.16$ ppm; $\delta(\text{CD}_2\text{Cl}_2) = 53.84$ ppm; $\delta(\text{DMSO-d}_6) = 39.52$ ppm) and CFCl_3 as external standard for ¹⁹F-NMR spectra. For column chromatography silica gel (0.035-0.070 mm, 60 Å pore size) was used. IR spectra (neat) were taken on a Bruker VERTEX 70v. The 6P reference spectrum was obtained for material obtained from TCI Europe.

Synthesis



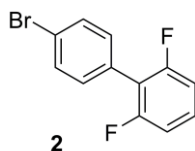
Scheme S1. Synthesis of target compounds *o*-2F-6P and *m*-2F-6P.

4-Bromo-3',5'-difluorobiphenyl 1



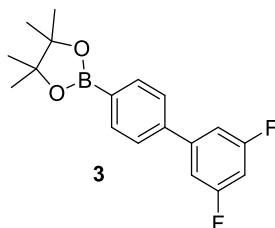
Argon was bubbled through a solution of 4-bromoiodobenzene (5.36 g, 19.0 mmol) in 1,2-dimethoxyethane (40 mL) for 10 min. Pd(PPh₃)₄ (0.44 g, 0.38 mmol), CsF (3.85 g, 25.3 mmol), Ag₂O (3.52 g, 15.2 mmol), and 3,5-difluorophenylboronic acid (2.00 g, 12.7 mmol) were added under an argon atmosphere. The suspension was stirred at 70 °C overnight and cooled to room temperature. After filtration over Celite® and washing with ethyl acetate, water was added and the mixture was extracted with ethyl acetate thrice. The combined organic layers were dried over anhydrous MgSO₄ and purified by silica gel column chromatography with petroleum ether to yield the product as white crystals (1.4 g, 5.2 mmol, 41%). ¹H-NMR (300 MHz, CDCl₃): δ [ppm]= 6.81 (tt, *J*=8.8 Hz, *J*=2.3 Hz, 1H), 7.06 (m, 2H), 7.41 (dt, *J*=8.6 Hz, *J*=2.3 Hz, 2H), 7.59 (dt, *J*=8.7 Hz, *J*=2.3 Hz, 2H). ¹³C{¹H}-NMR (75 MHz, CDCl₃): δ [ppm]= 103.0, 109.9, 123.0, 128.7, 132.3, 137.9, 143.4, 163.4. ¹⁹F-NMR (282 MHz, CDCl₃): δ [ppm]= -109.5 (t, *J*=8.5 Hz, 2F).

4-Bromo-2',6'-difluorobiphenyl 2



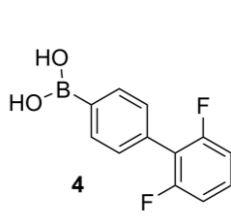
4-Bromo-iodobenzene (5.66 g, 20.0 mmol) was dissolved in 1,2-dimethoxyethane (70 mL). Argon and vacuum were applied alternately to the flask before addition of CsF (6.08 g, 40 mmol), Ag₂O (5.56 g, 24 mmol), 2,6-difluorophenylboronic acid (3.16 g, 20 mmol), and Pd(PPh₃)₄ (0.69 g, 0.6 mmol). After alternately applying vacuum and flushing with argon, the mixture was heated to 70 °C overnight. Upon cooling to room temperature the mixture was filtered over Celite® and washed with ethyl acetate. The organic layer was washed with water, dried over anhydrous MgSO₄ and evaporated under reduced pressure. The product **2** was obtained after silica gel column chromatography (petroleum ether) as a white solid (0.54 g) containing some terphenyl arising from two-fold coupling that was not further separated.

3,5-Difluoro-4'-(4,4,5,5-tetramethyl-1,3,2-dioxaborolan-2-yl)-biphenyl **3**



4-Bromo-3',5'-difluorobiphenyl **1** (1.00 g, 3.7 mmol) was dissolved in dry toluene (15 mL) under an argon atmosphere. Dry triethylamine (1.54 mL, 11.2 mmol), bis(triphenylphosphine)-palladium(II) chloride (52 mg, 0.07 mmol), and pinacolborane (0.81 mL, 5.6 mmol) were added. The solution was stirred for 19 h at 100 °C. Pinacolborane (0.81 mL, 5.6 mmol) was added again and the solution was stirred for 7 h. Ethyl acetate was added and the solution was washed with brine. The organic layer was dried over anhydrous MgSO₄ and the sample evaporated to dryness. Silica gel column chromatography (petroleum ether/ethyl acetate = 20/1) afforded **3** (0.27 g, 0.8 mmol, 23%) as a white solid. ¹H-NMR (300 MHz, DMSO-d₆): δ [ppm]= 1.30 (s, 12H), 7.25 (tt, *J*=9.3 Hz, *J*=2.3 Hz, 1H), 7.46 (m, 2H) 7.76 (m, 4H). ¹³C{¹H}-NMR (75 MHz, DMSO-d₆): δ [ppm]= 24.7, 83.8, 103.2, 109.9, 126.3, 135.1, 140.3, 143.4, 162.8. ¹⁹F-NMR (282 MHz, DMSO-d₆): δ [ppm]= -104.3 (t, *J*=8.9 Hz, 2F).

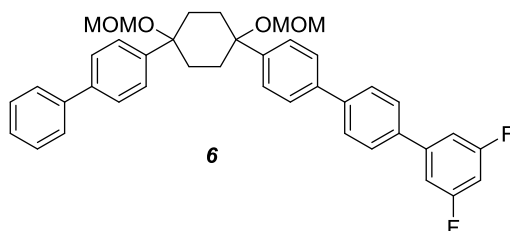
3,5-Difluorobiphenyl-4'-boronic acid **4**



Under an argon atmosphere the white solid **2** (0.54 g) was dissolved in dry THF and cooled to -78 °C. *n*-BuLi (2.2 M in cyclohexane, 1.1 mL, 2.4 mmol) was added and the mixture was stirred for 1 h at -78 °C. Triisopropyl borate (0.3 mL, 2.4 mmol) was added and the reaction was warmed to room temperature and stirred overnight. The mixture was acidified with 1 M aqueous HCl and extracted with dichloromethane. After evaporation of the organic layer, 1 M aqueous NaOH was added and the solution was washed with petroleum ether. Silica gel column chromatography

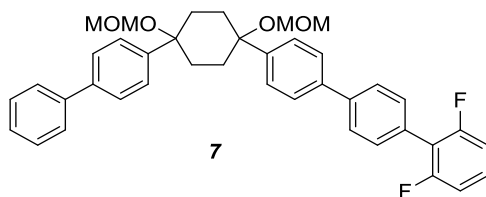
(dichloromethane/MeOH = 100/5) afforded a white solid (150 mg), which contains mostly the biphenylboronic acid **4** and was used without further purification.

m-2F-6P precursor **6**



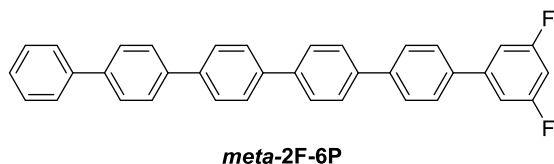
1-(4-Bromophenyl)-4-(biphenyl-4-yl)-1,4-bis(methoxymethoxy)cyclohexane **5** (380 mg, 0.75 mmol) and CsF (230 mg, 1.51 mmol) were suspended in 1,2-dimethoxyethane (10 mL). Argon was bubbled through the solution for 10 min and tris(dibenzylideneacetone)dipalladium chloroform adduct (20 mg, 0.02 mmol), tri-*tert*-butylphosphine (0.13 mL, 0.05 mmol, 10 wt% in hexane) and 3,5-difluoro-4'-(4,4,5,5-tetramethyl-1,3,2-dioxaborolan-2-yl)-biphenyl **3** (250 mg, 0.79 mmol) were added. The suspension was stirred for 20 h at 75 °C and filtered over Celite[®]. Water was added and the mixture was extracted with ethyl acetate. The organic layer was dried over anhydrous MgSO₄ and the solvent was evaporated under reduced pressure. Silica gel column chromatography (petroleum ether/ethyl acetate = 80/20) afforded the product **6** (220 mg, 0.35 mmol, 44%) as a white solid. ¹H-NMR (300 MHz, CD₂Cl₂): δ [ppm]= 2.16 (m, 4H), 2.37 (m, 4H), 3.41 (m, 6H), 4.47 (m, 4H), 6.83 (tt, *J*=9.0 Hz, *J*=2.3 Hz, 1H), 7.19 (m, 2H) 7.33 (tt, *J*=7.3 Hz, *J*=2.3 Hz, 1H), 7.43 (m, 2H) 7.62 (m, 14H). ¹³C{¹H}-NMR (75 MHz, DMSO-*d*₆): δ [ppm]= 19.1, 41.8, 64.0, 78.2, 88.5, 95.8, 123.6, 123.7, 123.7, 125.2, 126.2, 126.6, 126.7, 130.0, 130.1, 130.2, 149.4. ¹⁹F-NMR (282 MHz, DMSO-*d*₆): δ [ppm]= -104.3 (t, *J*=8.9 Hz, 2F).

o-2F-6P precursor **7**



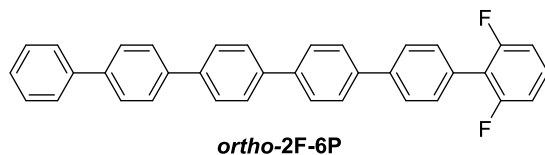
1-(4-Bromophenyl)-4-(biphenyl-4-yl)-1,4-bis(methoxymethoxy)cyclohexane **5** (328 mg, 0.64 mmol) and Pd(PPh₃)₄ (37 mg, 0.03 mmol) were dissolved in toluene (20 mL) and vacuum and argon were applied alternately 3x to the flask with stirring. After 15 min the crude boronic acid **4** (150 mg, dissolved in few droplets of EtOH) and 2 M aqueous Na₂CO₃ (1 mL) were added and vacuum and argon were applied alternately 3x again. The mixture was heated to reflux overnight. After cooling to room temperature water was added and the mixture was extracted with dichloromethane. The combined organic layers were dried over anhydrous MgSO₄ and evaporated under reduced pressure. Silica-gel column chromatography (petroleum ether/dichloromethane = 7/3) afforded the product **7** as a white solid (230 mg), which was further purified by recycling GPC to yield a white powder (126 mg, 0.2 mmol, 1% over 3 steps). ¹H-NMR (300 MHz, CDCl₃): δ [ppm]= 2.21 (m, 4H), 2.43 (m, 4H), 3.46 (m, 6H), 4.51 (m, 4H), 7.02 (m, 2H), 7.32 (m, 2H) 7.44 (m, 2H), 7.55 (m, 8H) 7.61 (m, 4H), 7.67 (m, 2H). ¹³C{¹H}-NMR (75 MHz, CD₂Cl₂): δ [ppm]= 33.6, 56.3, 78.5, 92.6, 92.7, 112.0, 127.4, 127.4, 127.4, 127.5, 127.9, 128.0, 128.0, 128.8, 131.2, 131.3, 140.0, 140.6, 141.0, 141.1. ¹⁹F-NMR (282 MHz, CD₂Cl₂): δ [ppm]= -115.5 (t, *J*=6.8 Hz, 2F).

***m*-2F-6P**



m-2F-6P precursor **6** (60 mg, 0.1 mmol) and *p*-toluenesulfonic acid (19 mg, 0.1 mmol) were suspended in xylenes (5 mL) and irradiated in a microwave (300 W) at 160 °C for 1 h. After cooling to room temperature and filtration the green solid residue was extensively washed with ethyl acetate, water, ethyl acetate, and methylene chloride. Gradient sublimation yielded the product as a greenish crystalline solid (32 mg, 0.08 mmol, 66%), containing minor amounts of the not completely aromatized product as discussed in Ref. 1. Fluorescence (CHCl₃, 25 °C) $\lambda_{\text{max,ex}}$ ($\lambda_{\text{em}} = 400 \text{ nm}$) = 320 nm, $\lambda_{\text{max,em}}$ ($\lambda_{\text{ex}} = 320 \text{ nm}$) = 382 nm, 398 nm. EI-MS [M]⁺ *m/z* calculated for C₃₆H₂₄F₂: 494.1846 found: 494.1846. EA calculated for C₃₆H₂₄F₂: C: 87.43%, H: 4.89% found: 86.54%, H: 5.08%. The slight disagreement between observed and calculated elemental composition is attributed to the hygroscopic nature of the sample.

***o*-2F-6P**



o-2F-6P precursor **7** (60 mg, 0.1 mmol) and *p*-toluenesulfonic acid (19 mg, 0.1 mmol) were suspended in xylenes (5 mL) and irradiated in a microwave (300 W) at 160 °C for 1 h. After cooling to room temperature and filtration the green solid residue was extensively washed with ethyl acetate, water, ethyl acetate, and methylene chloride. Gradient sublimation yielded the product as a greenish crystalline solid (30 mg, 0.08 mmol, 62%), containing minor amounts of the not completely aromatized product as discussed in Ref. 1. Fluorescence (CHCl₃, 25 °C) $\lambda_{\text{max,ex}}$ ($\lambda_{\text{em}} = 376 \text{ nm}$) = 312 nm, $\lambda_{\text{max,em}}$ ($\lambda_{\text{ex}} = 312 \text{ nm}$) = 376 nm, 391 nm. EI-MS [M]⁺ *m/z* calculated for C₃₆H₂₄F₂: 494.1846 found: 494.1846. EA calculated for C₃₆H₂₄F₂: C: 87.43%, H: 4.89% found: 86.12%, H: 5.03%. The slight disagreement between observed and calculated elemental composition is attributed to the hygroscopic nature of the sample.

^1H and ^{13}C NMR spectra of intermediates and precursors

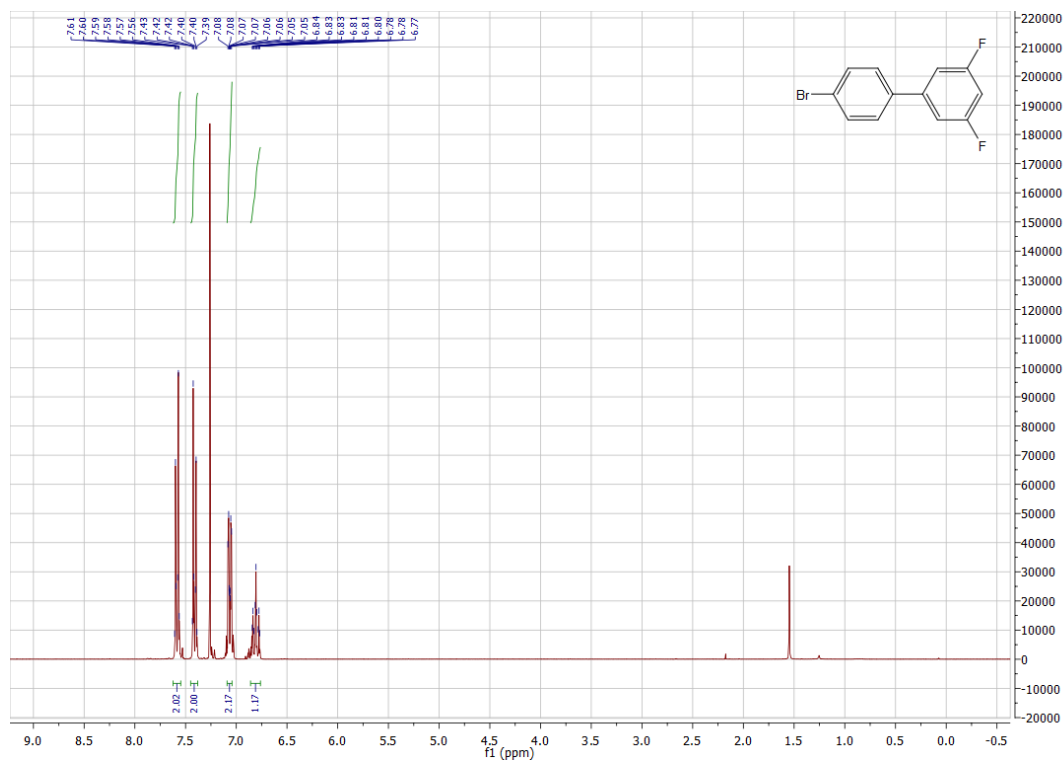


Figure S3. ^1H -NMR spectrum of **1** in CDCl_3 at $25\text{ }^\circ\text{C}$.

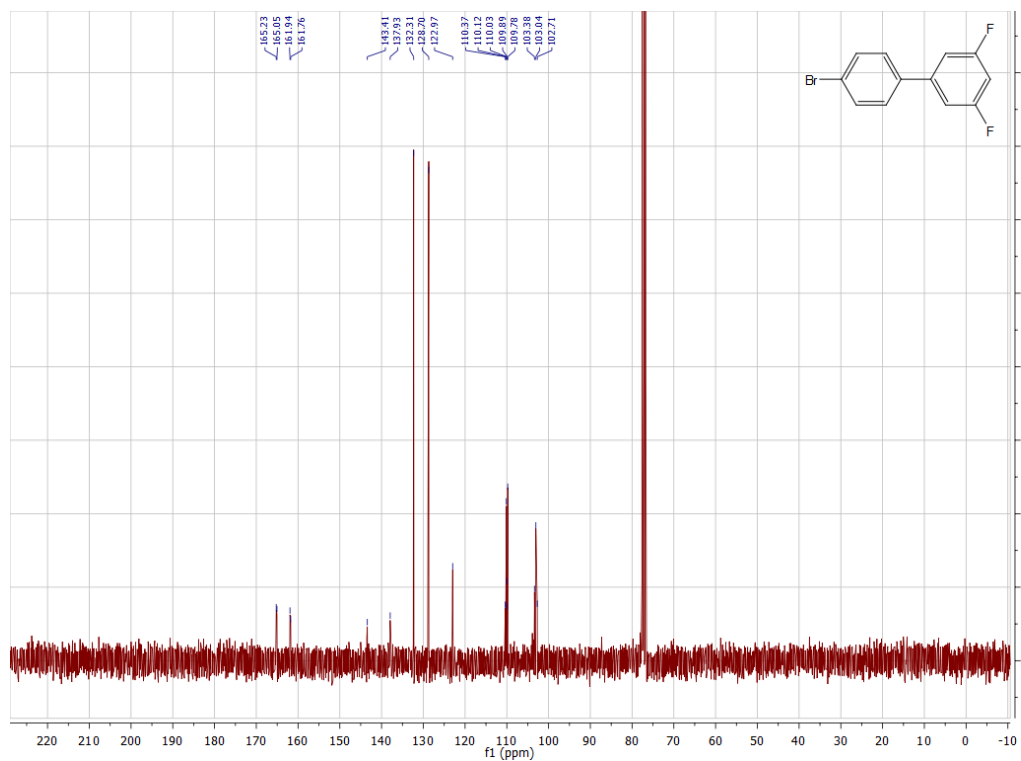


Figure S4. ^{13}C -NMR spectrum of **1** in CDCl_3 at $25\text{ }^\circ\text{C}$.

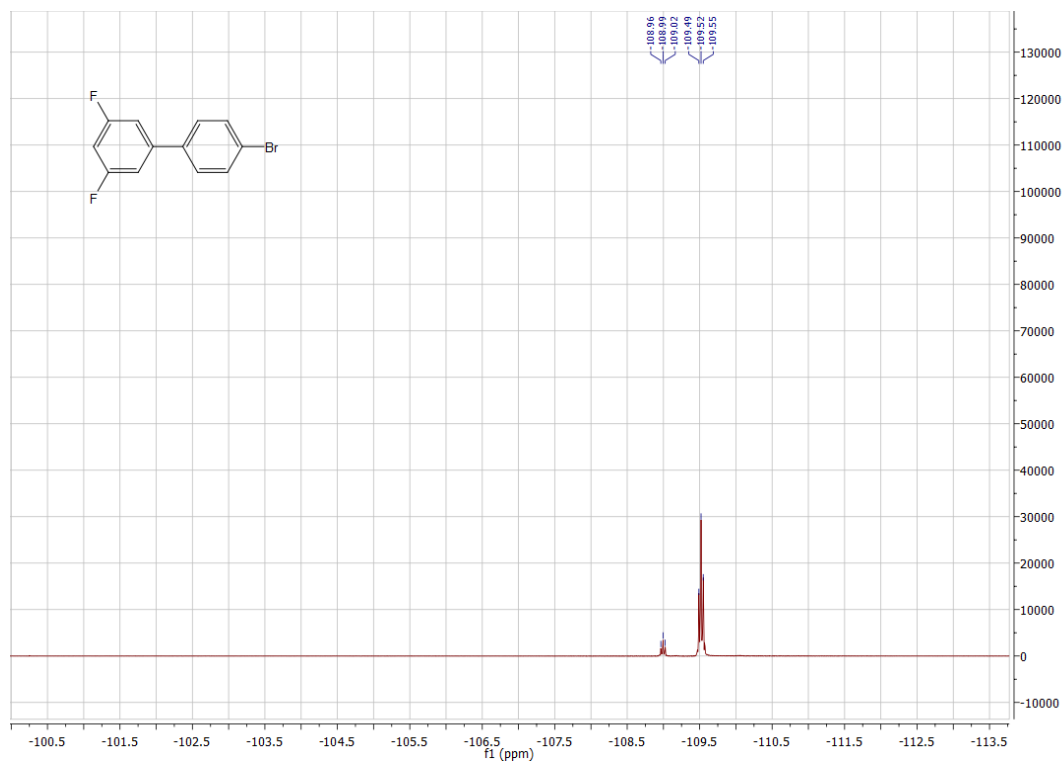


Figure S5. ^{19}F -NMR spectrum of **1** in CDCl_3 at $25\text{ }^\circ\text{C}$.

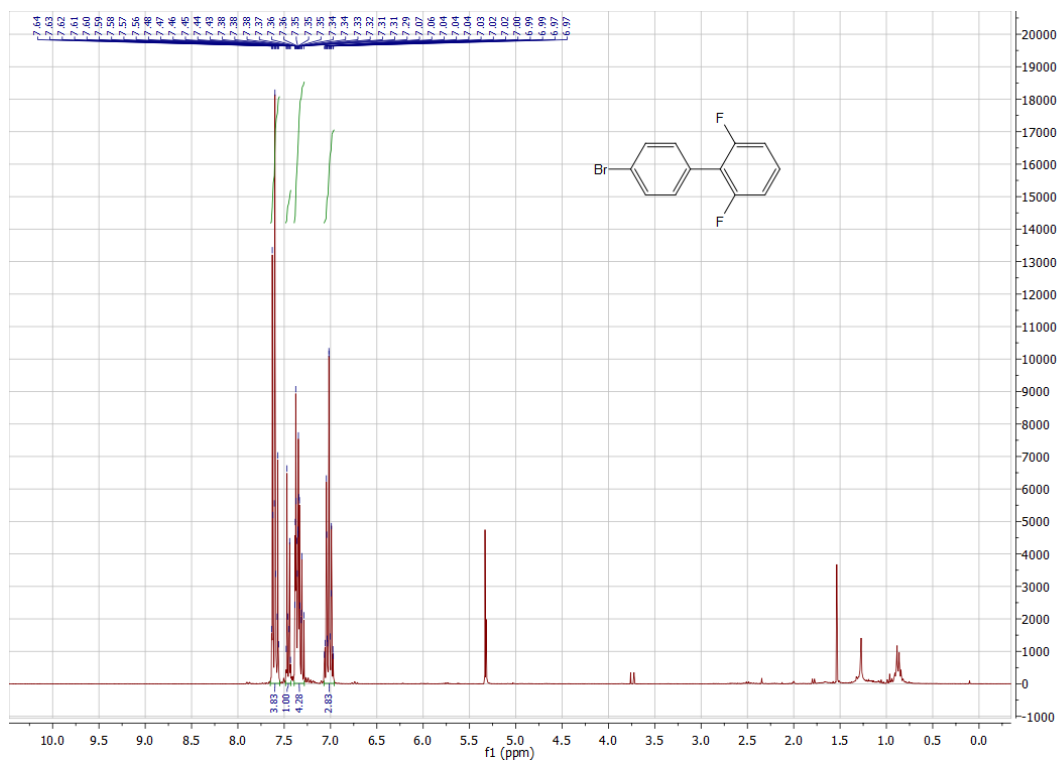


Figure S6. ^1H -NMR spectrum of **2** in CD_2Cl_2 at $25\text{ }^\circ\text{C}$.

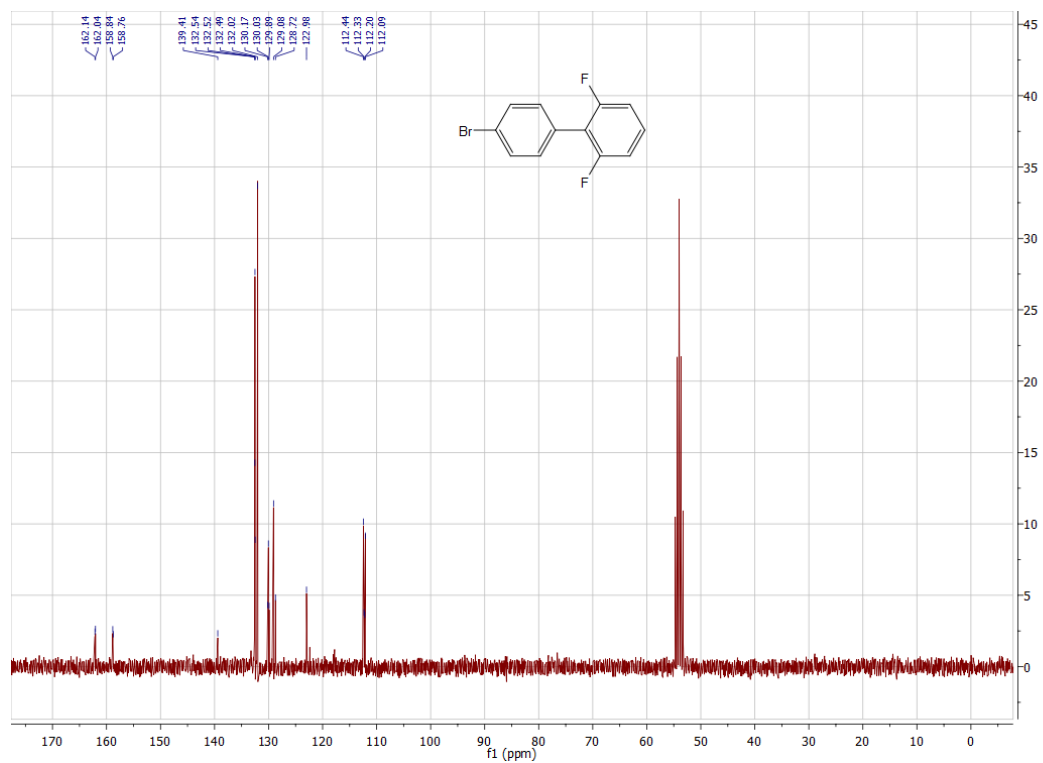


Figure S7. $^{13}\text{C-NMR}$ spectrum of **2** in CD_2Cl_2 at 25 °C.

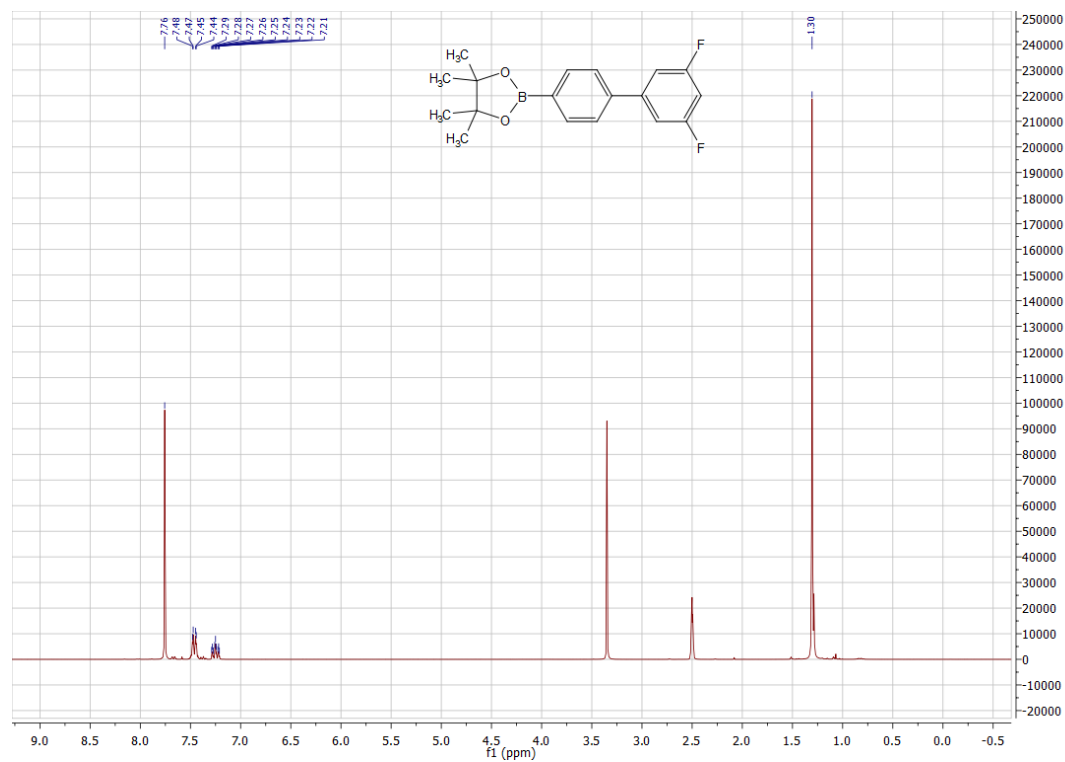


Figure S8. $^1\text{H-NMR}$ spectrum of **3** in DMSO-d_6 at 25 °C.

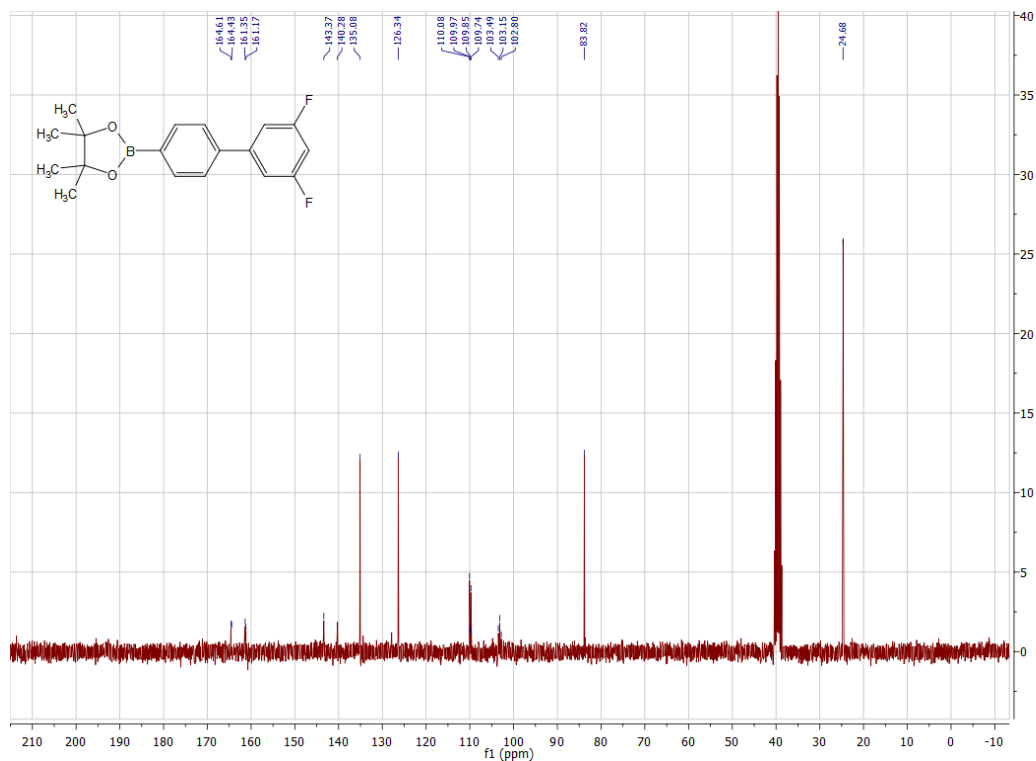


Figure S9. ^{13}C -NMR spectrum of **3** in DMSO-d_6 at $25\text{ }^\circ\text{C}$.

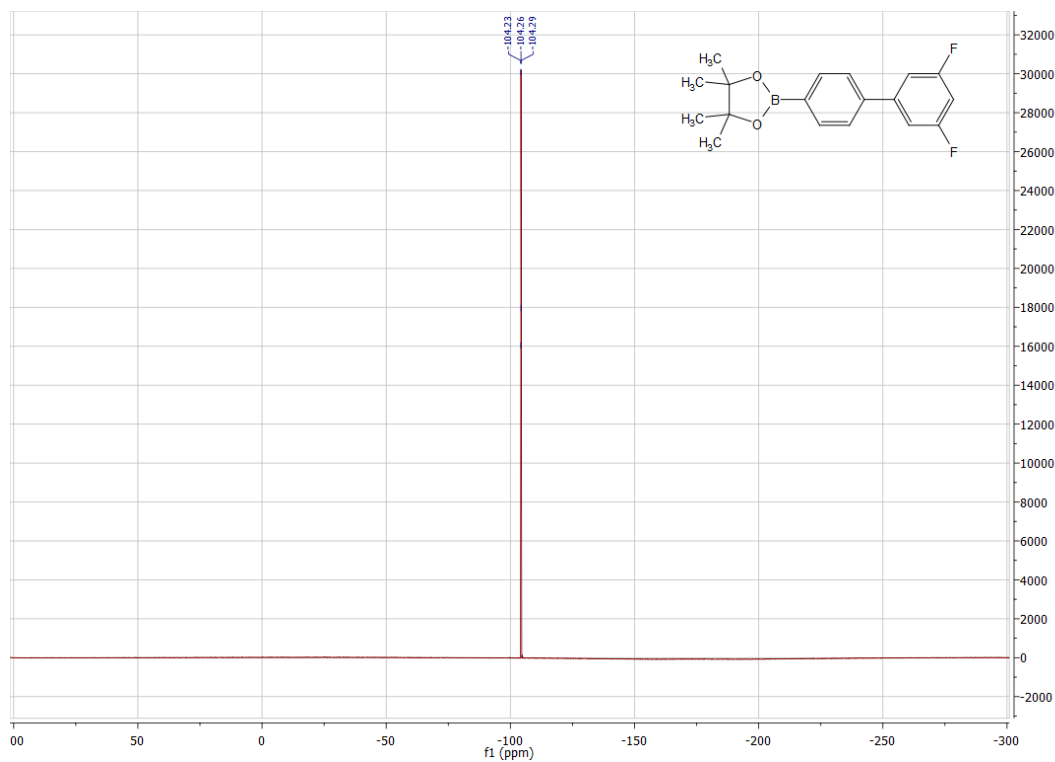


Figure S10. ^{19}F -NMR spectrum of **3** in DMSO-d_6 at $25\text{ }^\circ\text{C}$.

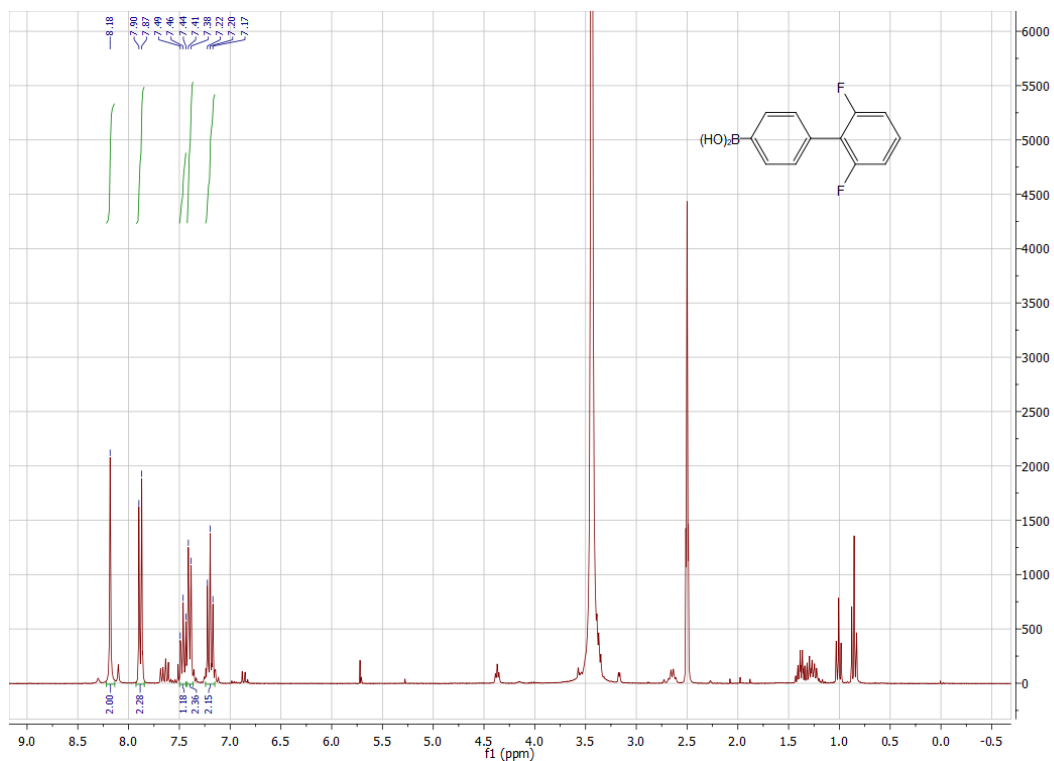


Figure S11. $^1\text{H-NMR}$ spectrum of **4** in DMSO-d_6 at $25\text{ }^\circ\text{C}$.

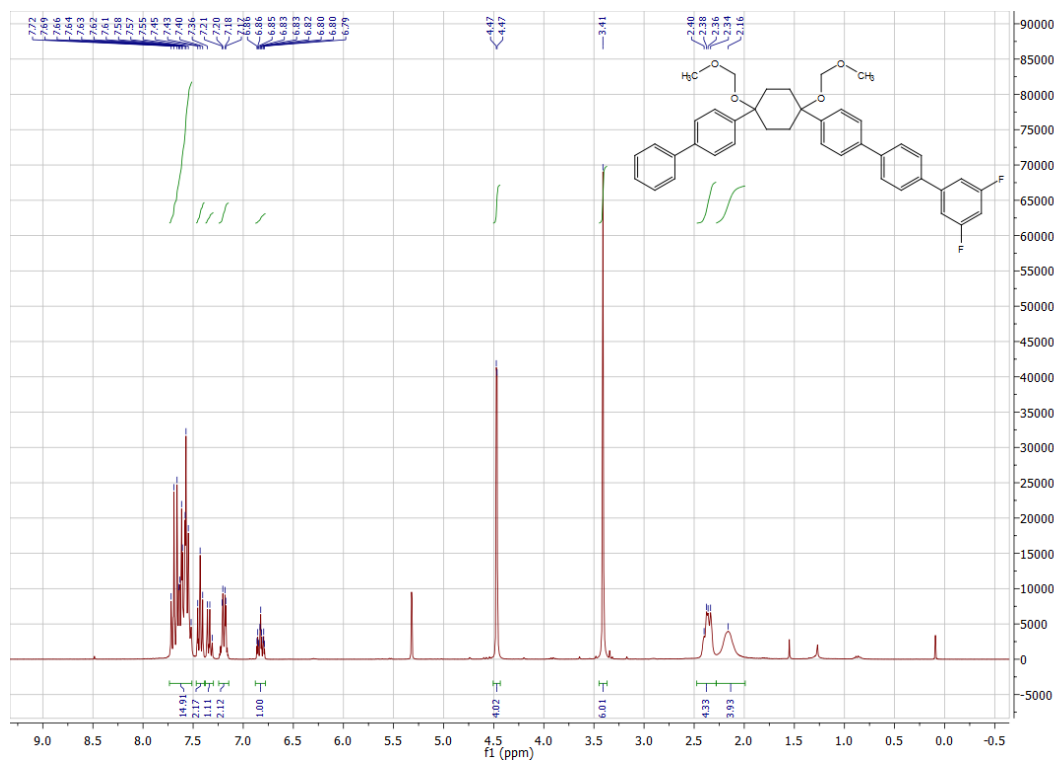


Figure S12. $^1\text{H-NMR}$ spectrum of **6** in CD_2Cl_2 at $25\text{ }^\circ\text{C}$.

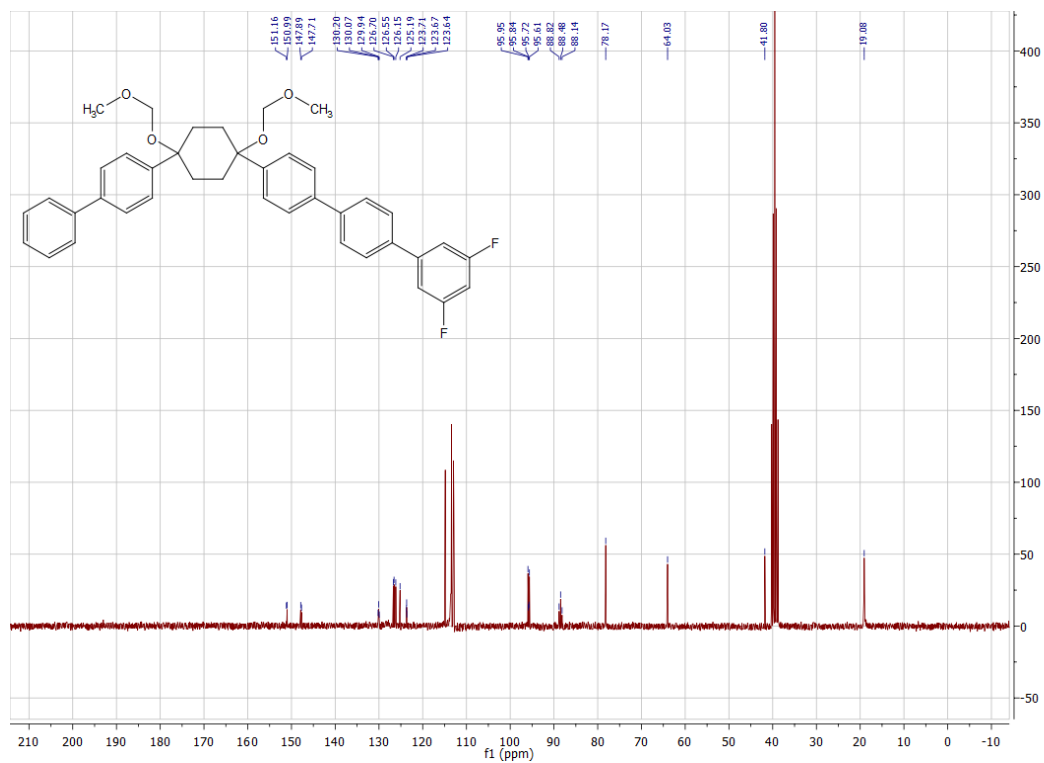


Figure S13. ^{13}C -NMR spectrum of **6** in DMSO-d_6 at $25\text{ }^\circ\text{C}$.

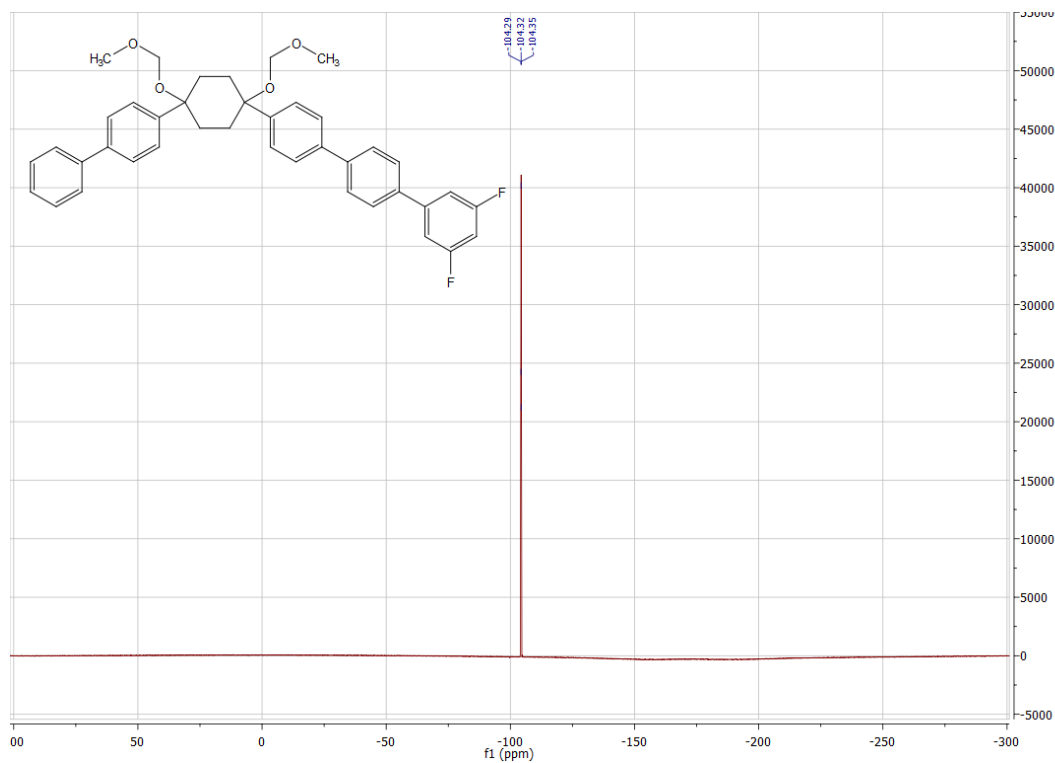


Figure S14. ^{19}F -NMR spectrum of **6** in CD_2Cl_2 at $25\text{ }^\circ\text{C}$.

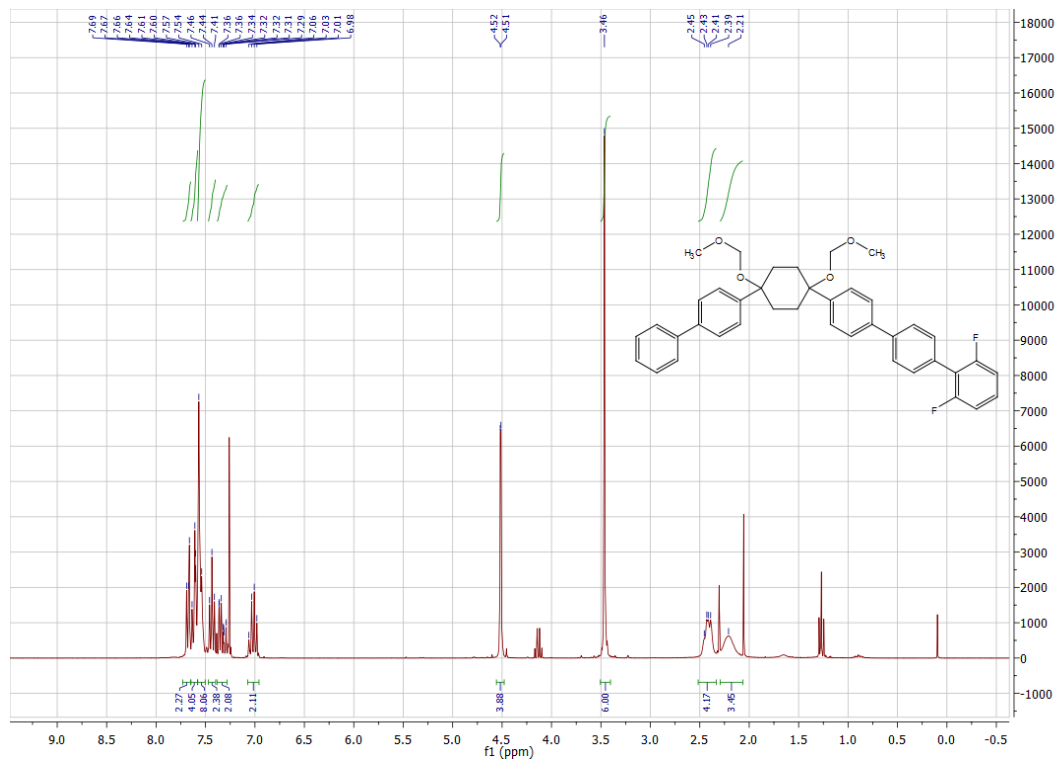


Figure S15. ¹H-NMR spectrum of **7** in CD₂Cl₂ at 25 °C.

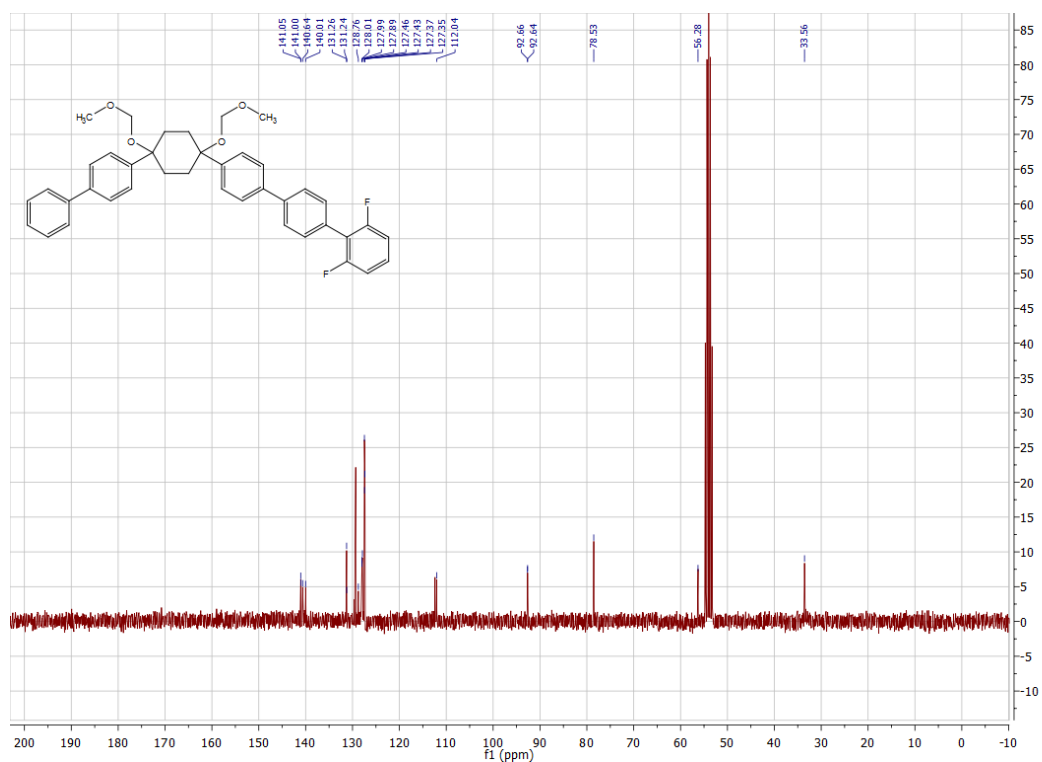


Figure S16. ¹³C-NMR spectrum of **7** in CD₂Cl₂ at 25 °C.

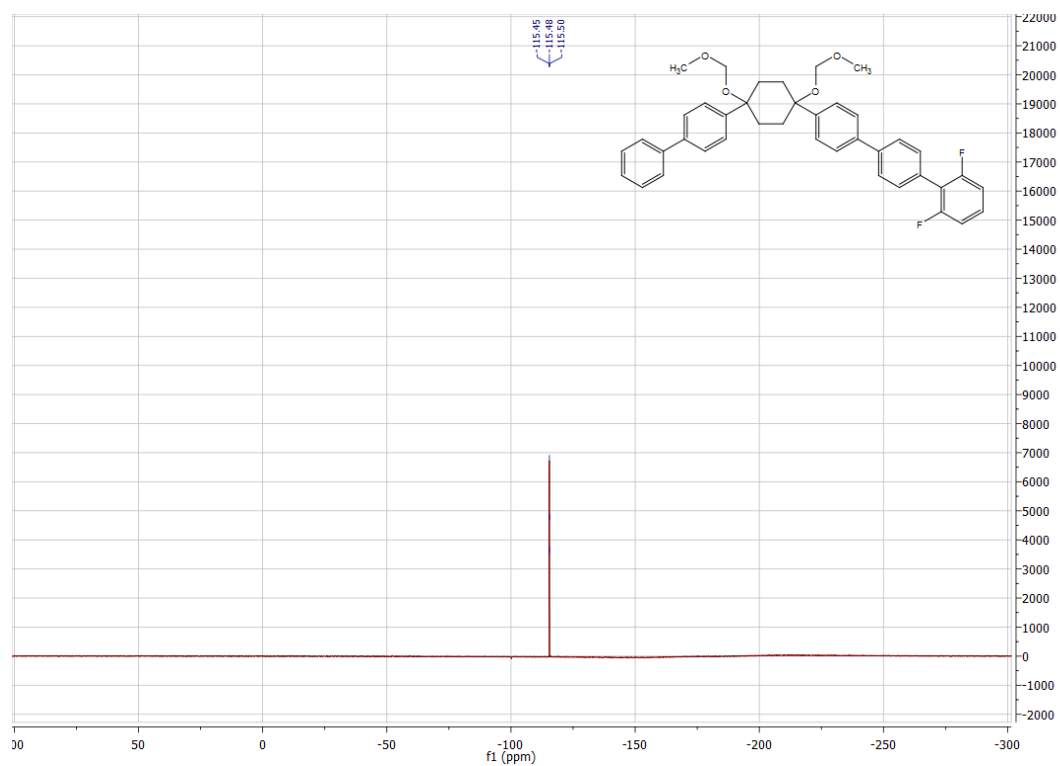


Figure S17. ^{19}F -NMR spectrum of **7** in CD_2Cl_2 at $25\text{ }^\circ\text{C}$.

IR Spectra of the final compounds

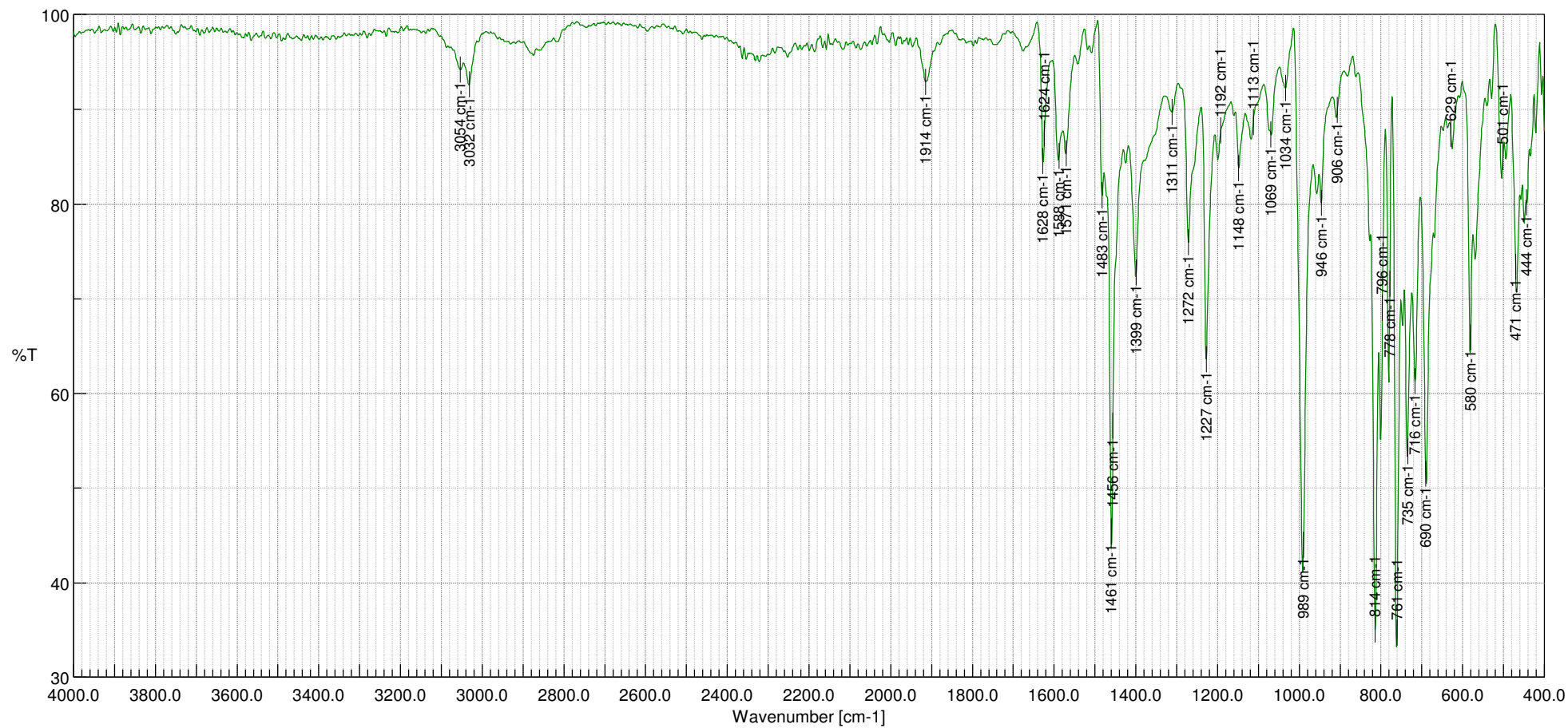


Figure S18. IR spectrum of *o*-2F-6P (neat)

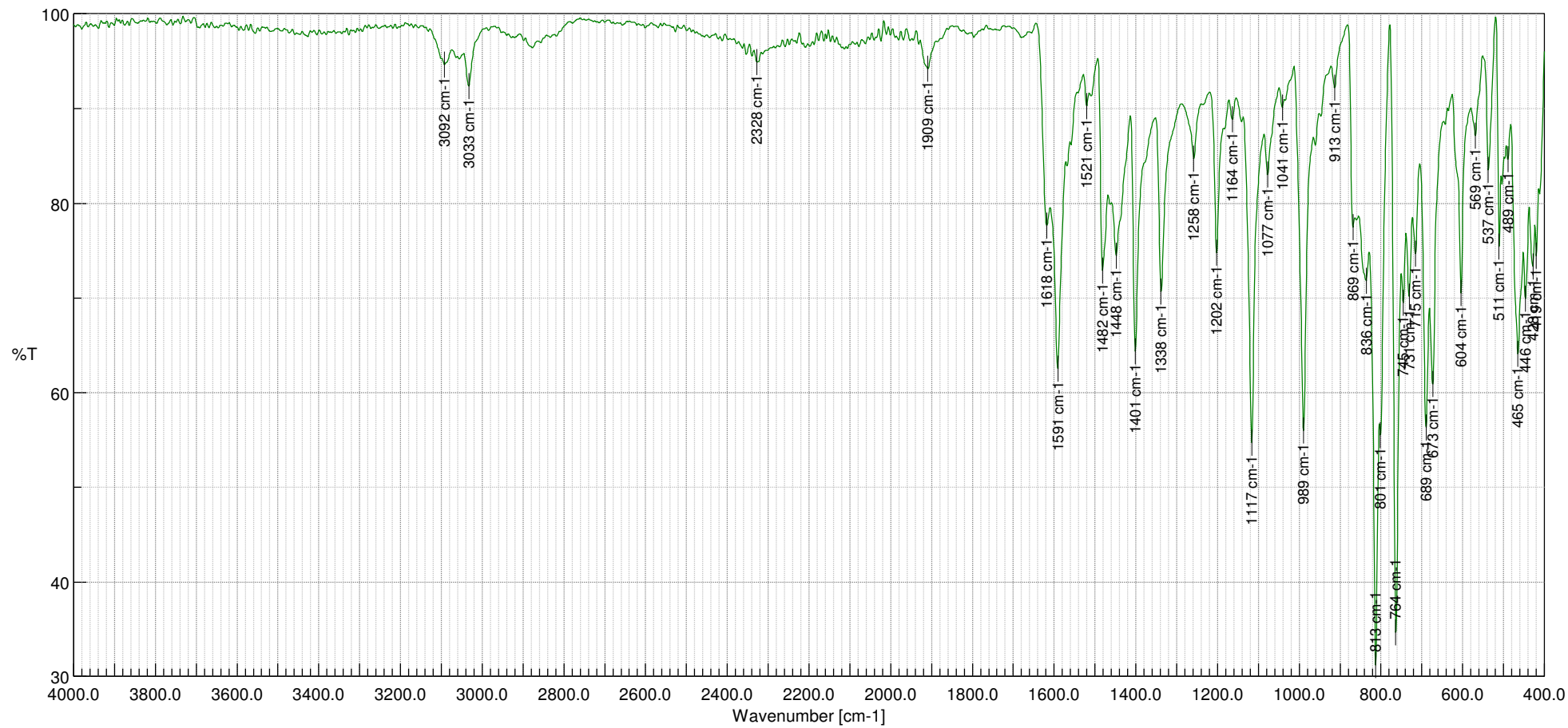


Figure S19. IR spectrum of *m*-2F-6P (neat)

IR Spectrum of 6P reference

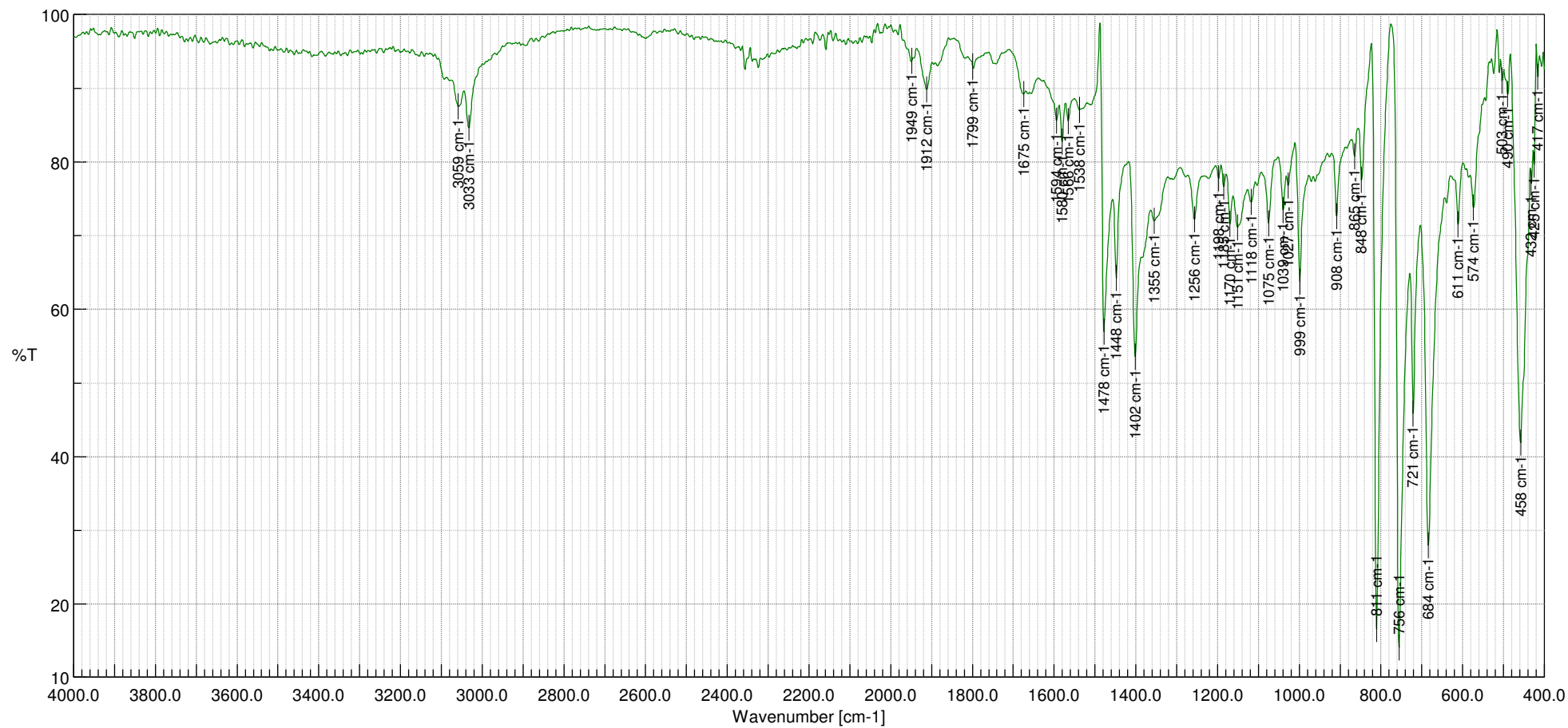


Figure S20. IR spectrum of 6P (neat)

Molecular arrangement of 6P deposited at ca. 70 K

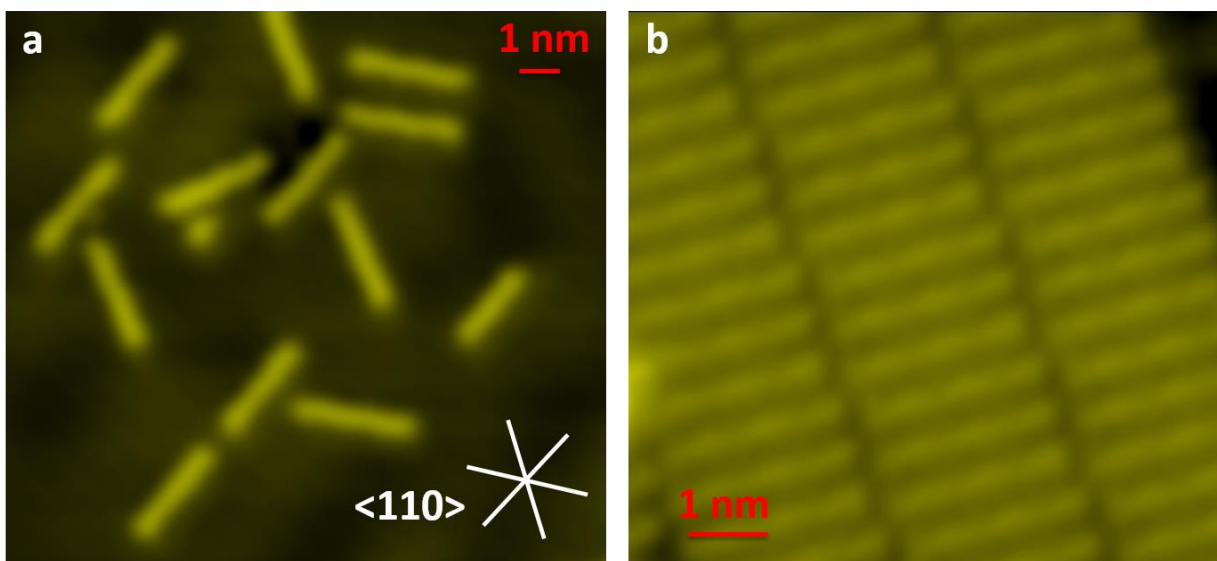


Figure S21. STM images of 6P deposited onto Ag(111) at ca. 70 K sample temperature. (a) and (b) show isolated molecules for low coverage and molecular arrays around monolayer coverage, respectively [$V = -2$ V, $I = 55$ pA].

Scanning tunneling spectroscopy results for *m*-2F-6P

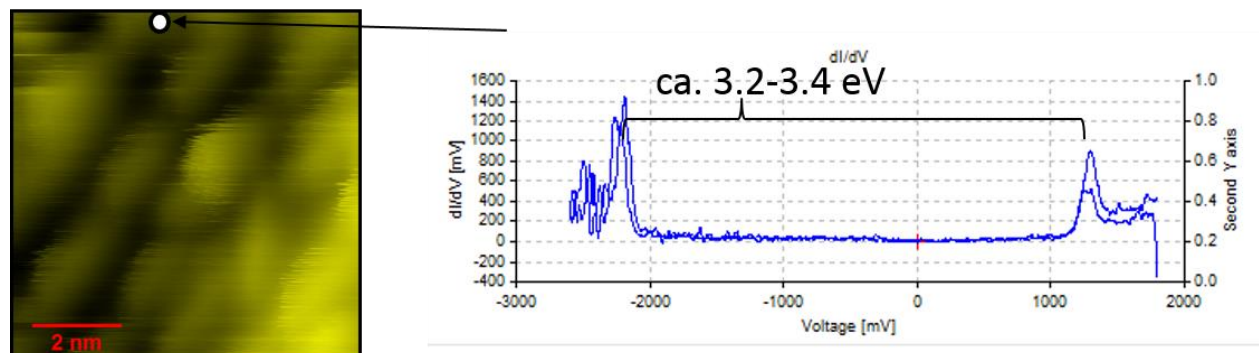


Figure S22. Left: STM image of the aggregated *m*-2F-6P/Ag(111) molecules used for the STS experiments. [V = 1 V, I = 50 pA, 7.1 nm x 7.1 nm scan] **Right:** STS data (overlaid forward and backward scan) showing energetic position of HOMO (at negative voltage) and LUMO (at positive voltage). [Conditions for approach: V = 1.8 V, I = 50 pA]

Fig. S22 shows scanning tunneling spectroscopy (STS) results for *m*-2F-6P/Ag(111). As can be seen, the Fermi level is located well inside the HOMO-LUMO gap of *m*-2F-6P, consistent with physisorption of both 6P derivatives when adsorbed on Ag(111). The significant smaller energetic difference between the LUMO level and Fermi level, compared to that of the HOMO level, is consistent with a minute electron transfer *towards* the molecules.

Manipulation of a canted arrangement with the STM tip

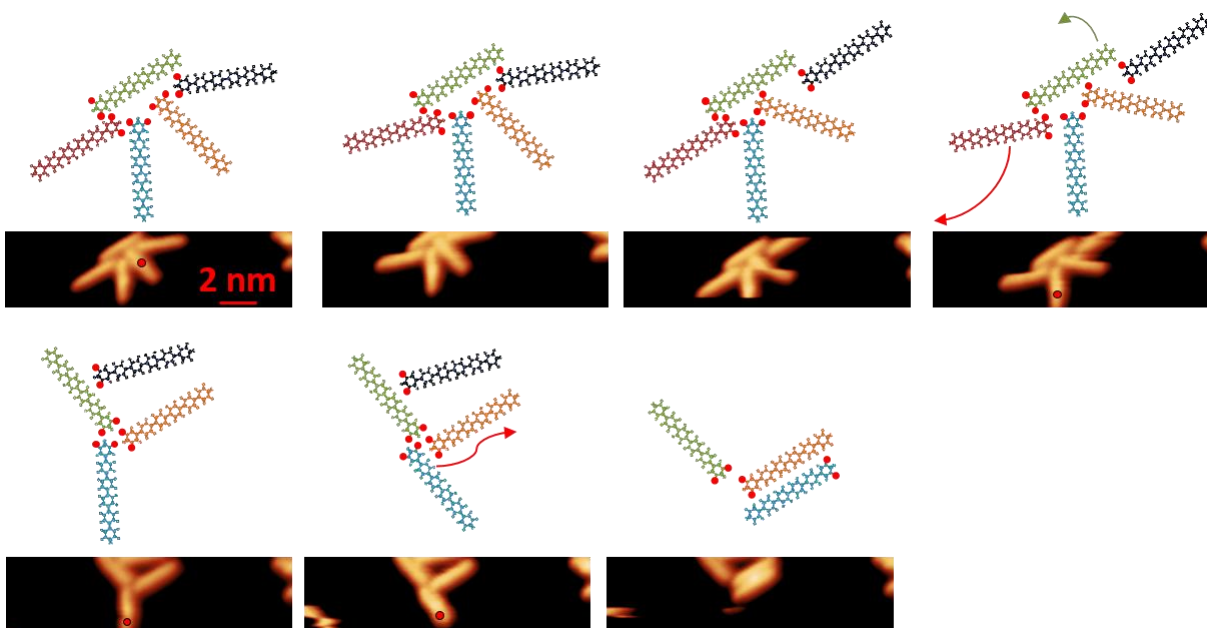


Figure S23. A cluster of m-2F-6P molecules exhibiting a canted arrangement that undergoes repeated changes in the molecules' docking direction induced by the normal scanning process and deliberate voltage pulses applied with the STM tip. The rearrangements proceeded from the configuration in the top left, which was found to be stable for several scans and several short pulses, to the right bottom. Pulses are indicated by red dots that indicate the approximate position the pulse was applied at. [$V = -1$ V, $I = 0.58$ nA, 15.4 nm x 4 nm scans. The first four pulses employed a -1 V bias that was applied for 18 s (for the first) or 30 s (for pulses 2 – 4) with the feedback loop turned off. The last pulse was at -1.5 V for 15 s.].

Line profiles for *m*-2F-6P

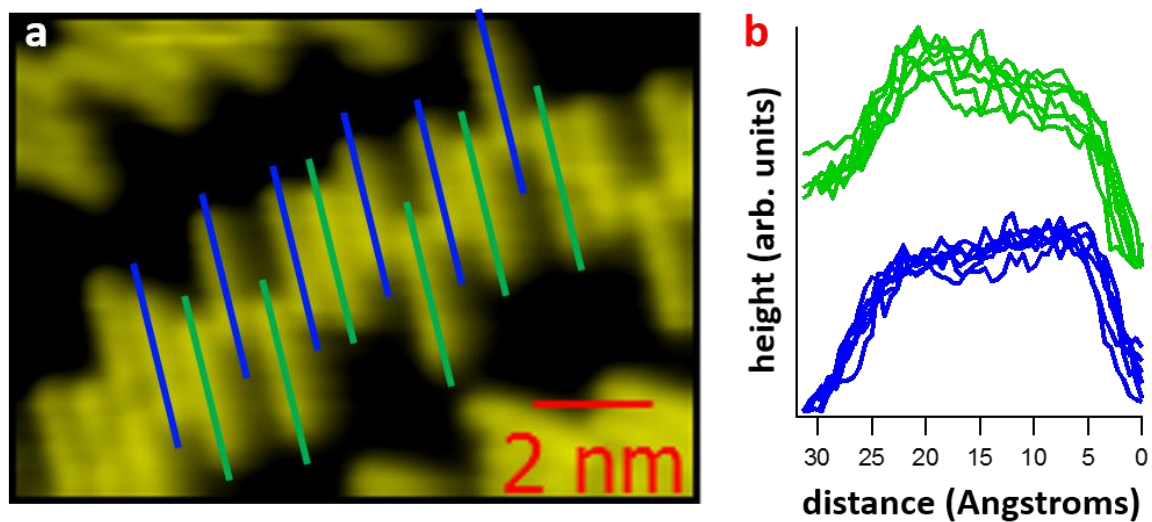


Figure S24. (a) STM image of a zipper arrangement. [$V = -1019$ mV, $I = 0.10$ nA, 30.4 nm x 23.3 nm scan].

(b) Line scans taken along the lines indicated in (a) (starting point: top left).

Crystal structure of *m*-4F-6P

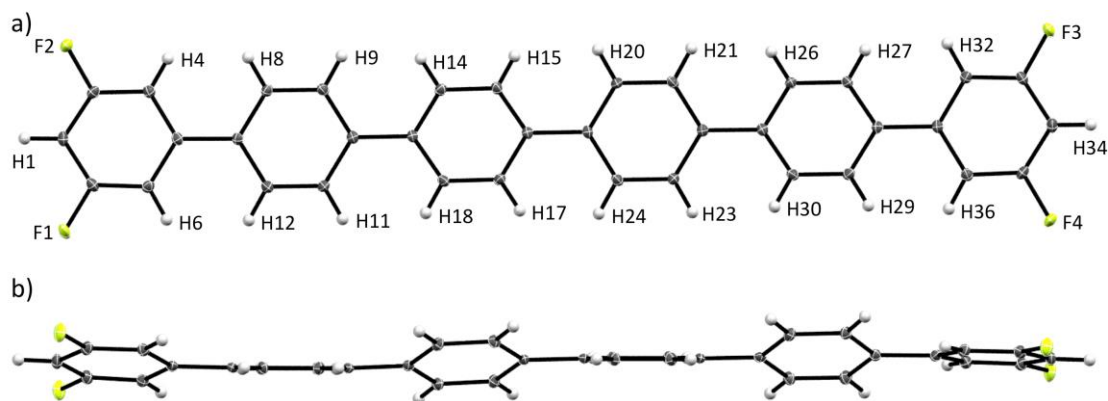


Figure S25. One independent molecule of *o*-4F-6P with thermal ellipsoids at the 50% probability level in (a) top view and (b) side view.

The symmetrically substituted *m*-4F-6P was crystallized by slow sublimation in a custom-made plate sublimation apparatus.² The prepared single-crystal was mounted using a microfabricated polymer film crystal-mounting tool (dual-thickness MicroMount, MiTeGen) and low viscosity oil (perfluoropolyalkylether; viscosity 1800 cSt, ABCR) to reduce the X-ray absorption and scattering. A Bruker D8 Venture single-crystal X-ray diffractometer with area detector using Mo- K_{α} ($\lambda = 0.71073 \text{ \AA}$) radiation was used for data collection at -173 ° . Multiscan absorption corrections implemented in SADABS³ were applied to the data. The structure was solved by intrinsic phasing (SHELXT-2013)⁴ and refined by full-matrix least-squares methods on F^2 (SHELXL-2014).⁵ *m*-4F-6P shows systematic twinning, the structure was therefore refined as a twin. The hydrogen atoms were placed at calculated positions and refined by using a riding model. CCDC 1833532 (*m*-4F-6P) contains the supplementary crystallographic data for this paper. These data can be obtained free of charge from The Cambridge Crystallographic Data Centre.

m-4F-6P was assigned as P-1 space group with two independent molecules in the asymmetric unit. The crystal structure was solved as twin and refined accordingly. Upon completion, checkcif suggests a higher symmetry, which is not valid according to Platon/ADDSYM. The space group was retained as P-1.

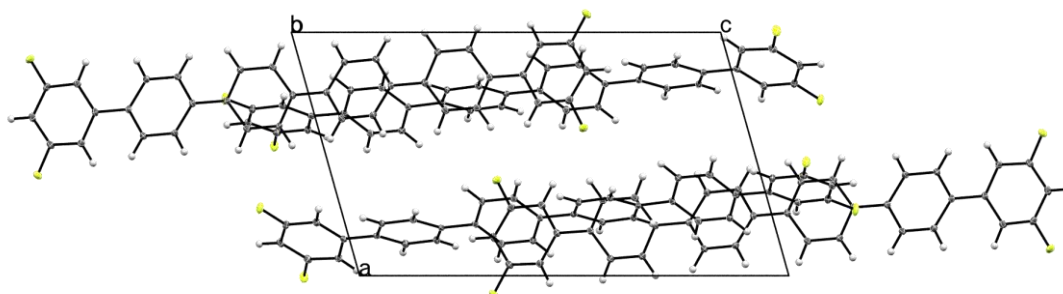


Figure S26. View of the unit cell of *m*-4F-6P along the crystallographic *b* axis.

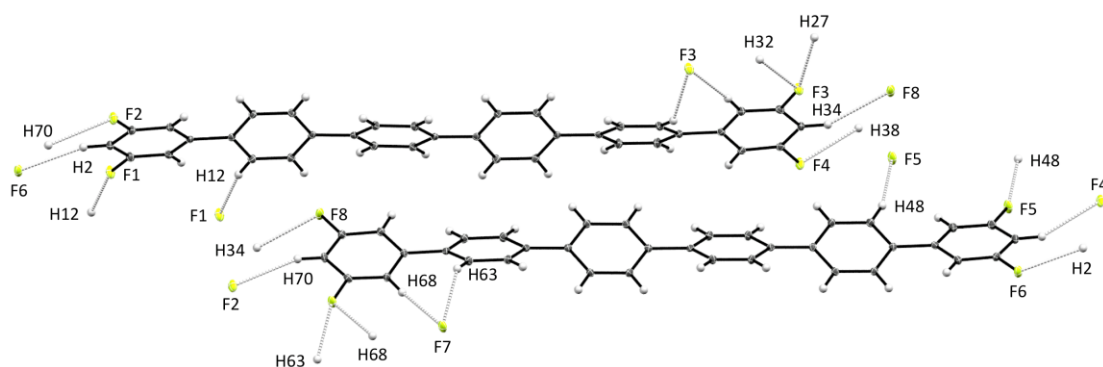


Figure S27. Intermolecular C-H...F contacts of the asymmetric unit of *m*-4F-6P along the crystallographic *b* axis.

Table S3. Intermolecular C-H...F contacts of the asymmetric unit of *m*-4F-6P. Angles are determined between C,H,F atoms, C the being the carbon of the donor group.

Atoms	Contact Length [Å]	Contact Angle [°]
F1...H12	2.43	162.5
F2...H70	2.56	158.2
F3...H27	2.47	142.8
F3...H32	2.61	175.1
F4...H38	2.67	147.1
F5...H48	2.41	162.3
F6...H2	2.51	157.0
F7...H63	2.54	143.3
F7...H68	2.55	173.6
F8...H34	2.67	148.0

References

- [1] Garmshausen, Y., Schwarz, J., Hildebrandt, J., Kobin, B., Pätzelt, M., Hecht, S. Making Nonsymmetrical Bricks: Synthesis of Insoluble Dipolar Sexiphenyls *Org. Lett.* **2014**, *16*, 2838-2841.
- [2] *Charge-Carrier Mobility in Organic Crystals*; Farchioni, R., Grosso, G., Eds.; Springer Berlin Heidelberg, 2001; pp 283-326.
- [3] Sheldrick, G. M. SADABS, program for empirical absorption correction of area detector data, University of Göttingen, Göttingen, 1996.
- [4] Sheldrick, G. M. *SHELXT-2013*, Program for Crystal Structure Solution, University of Göttingen, Göttingen, 2013.
- [5] Sheldrick, G. M. *SHELXL-2014*, Program for Crystal Structure Refinement, University of Göttingen, Göttingen, 2014.